Knockdown of Dnmt1 links Gene body DNA methylation to regulation of gene expression and maternal-zygotic transition in the wasp *Nasonia*

Deanna Arsala[1,2], Xin Wu[3], Soojin V. Yi[3], and Jeremy A. Lynch[1]

[1] Department of Biological Sciences, University of Illinois at Chicago, Chicago IL

[2] Dept. of Ecology & Evolution, University of Chicago, Chicago IL

[3] School of Biological Sciences, Georgia Institute of Technology, Atlanta GA

Abstract

Gene body methylation (GBM) is an ancestral form of DNA methylation whose role in development has remained unclear. Unlike vertebrates, DNA methylation is found exclusively in gene bodies in the wasp *Nasonia vitripennis*, which provides a unique opportunity to interpret the role of GBM in development. We confirmed that parental RNAi (pRNAi) knockdown of a DNMT1 ortholog (*Nv-Dnmt1a*) in *Nasonia* leads to embryonic lethality and failures in cellularization and morphogenesis. Using whole-genome bisulfite sequencing, we found a widespread loss of GBM in *Nv-Dnmt1a* pRNAi embryos. Using RNAseq, we found that methylated genes that lost GBM in the pRNAi samples were exclusively downregulated during zygotic genome activation. Unexpectedly, nearly all affected unmethylated genes were up-regulated after pRNAi. Lack of proper clearance of mRNAs and abnormal activation drive this up-regulation, indicating critical roles for *Nv-Dnmt1a* and GBM in the maternal-zygotic transition (MZT) in the wasp, despite their absence in *Drosophila*.

Background

The maternal-zygotic transition (MZT) is an essential stage in multicellular eukaryotic development and represents the transition of developmental control <u>from</u> maternal genome products provided to the egg during oogenesis <u>to</u> the products of newly formed zygotic genome [1, 2]. A major hallmark of the handover to zygotic control is the coordination of the highly regulated decay of maternal mRNAs with the activation of transcription from the zygotic genome.

46 The interactions between the maternal and zygotic genome have been
47 most comprehensively demonstrated in the insect model *Drosophila*
48 *melanogaster*. Maternal transcript destabilization is carried out in part by
49 maternally deposited mRNAs encoding RNA binding proteins (RBPs) such as
50 *smaug* and *brain tumor* (*brat*) [3, 4]. These factors are aided by the transcription
51 factor Zelda (Zld), which promotes miRNA expression that further destabilize
52 maternal transcripts. Under normal circumstances Zld also increases chromatin
53 accessibility and helps activate thousands of zygotic genes to their proper level [5,
54 6, 7]. However, if clearance of maternal transcripts is impeded, the zygotic genome
55 is not properly activated. Thus, disruption of either zygotic genome activation, or
56 maternal transcript clearance leads to embryonic lethality. In both cases death is
57 due to failures in the earliest developmental events that are dependent on the
58 zygotic genome: cellularization of the syncytial blastoderm, and gastrulation [5, 8] .
59 Most of the strategies for regulating the *D. melanogaster* ZGA (e.g.,
60 histone modification, chromatin packaging, action of miRNAs, mRNA
61 degradation), and many of the molecules involved, are conserved throughout the
62 animals [9]. However, *D. melanogaster* lacks a major class of genomic regulation,
63 in the form of methylation of cytosines in CpG dinucleotides (CpG methylation) [10,
64 11]. CpG methylation is crucial for regulating gene expression in most complex
65 eukaryotes [12, 13], and has a significant role in regulating the MZT in many species
66 [14, 15]. Thus, its absence in *D. melanogaster*, and in the other major invertebrate
67 model system *C. elegans*, makes it difficult to elucidate the molecular
68 mechanisms of DNA methylation in early development.

69 CpG methylation is catalyzed by DNA methyltransferases 1 and 3
70 (DNMT1 and DNMT3), which are conserved and ancient components of the
71 eukaryotic genomic toolkit [16], but have been lost in Dipterans, including *D.*
72 *melanogaster* [17, 18]. However, both DNMT1 and 3 orthologs are found in many
73 other insect taxa including hemimetabolous insects [19] and within the
74 holometabolous lineage Hymenoptera [20, 21, 22, 23].
75 The most well understood functional impact of CpG methylation,
76 elucidated from studies of mammalian model system, is in silencing gene
77 expression via methylation of cis-regulatory sequences, particularly of normally
78 unmethylated clusters of CpGs (CpG islands) [13, 24]. However it is becoming clear
79 that cis-regulatory regulation at CpG islands is not a ubiquitous mechanism [25]. A
80 more universal, and likely ancestral [20, 26], form of DNA methylation occurs
81 between the transcription start site and transcription end site of a gene, and is
82 known as gene body methylation (**GBM**) [27].
83 Previous studies have correlated GBM with stable and higher levels of
84 gene expression than genes without GBM [26, 28, 29, 30, 31], but its role in regulating
85 gene expression in specific developmental contexts such as the MZT is poorly
86 understood. Whole-genome bisulfite sequencing (WGBS) studies have shown
87 that DNA methylation patterns are dynamic during the MZT in vertebrate model
88 systems [32, 33, 34]. However, such methylation studies in vertebrates have focused
89 on cis-regulatory regions, including CpG islands in promoters and intergenic
90 regions. Disruption of methylation at CpG islands often has profound phenotypic
91 effects, while the role of GBM is less well understood. Because manipulating

92 DNA methylation machinery in vertebrate models affects both CpG islands and
93 GBM, it is difficult to identify functions of GBM that are independent of CpG
94 island methylation.

95 In contrast to vertebrates, DNA methylation occurs almost exclusively at
96 gene bodies in insects that have retained DNA methyltransferases 1 and 3
97 (DNMT1 and DNMT3) [19, 22, 35, 36]. Thus, such insect model systems have the
98 potential to make significant contributions in understanding the role of GBM in
99 development. A particularly attractive system with a full methylation toolkit and
100 exclusively gene body methylation is the wasp *Nasonia vitripennis* [36, 37, 38].

101 There are three DNMT1 paralogs in the *N. vitripennis* genome, and one of
102 them, *Nv-DNA methyltransferase 1a* (*Nv-Dnmt1a*), was shown to be essential for
103 embryogenesis (the other two showed no obvious phenotype)[39]. Therefore, *N.*
104 *vitripennis* offers an exciting opportunity to functionally study the specific role of
105 gene body methylation in a well-defined developmental system. In this work, we
106 set out to experimentally investigate the role of *Nv-Dnmt1a* and thus identify a
107 role for gene body methylation in early embryogenesis of *N. vitripennis*.

108 Our detailed analysis of the developmental effects of *Nv-Dnmt1a* revealed
109 major defects in cellularization and morphogenesis of the early embryo, which
110 are phenotypes typically seen after disruption of the MZT in insects. Using
111 parental RNAi (pRNAi) and WGBS we found that the vast majority of gene body
112 methylation is lost when *Nv-Dnmt1a* is knocked down. We then show that loss of
113 gene body methylation during zygotic genome activation is correlated with
114 reduced gene expression from the affected locus during zygotic genome

115 activation. Furthermore, we found that genes that are not methylated, but whose
116 expression changed after *Nv-Dnmt1a* knockdown, were primarily upregulated in
117 knockdown embryos relative to control. *Nv-Dnmt1a* knockdown profoundly
118 altered the levels of expression of thousands of genes in the early embryo.
119

120 **Results**

121 ***Nv-Dnmt1a function is required for early embryonic events that require***
122 ***proper regulation of the zygotic genome***

123 The initial characterization of *Nv-Dnmt1a* showed that knockdown through
124 parental RNAi (pRNAi), where female embryos are injected with dsRNA [40], led to
125 lethality of embryos produced by injected females [39]. Understanding the precise
126 developmental failure(s) that lead to embryonic lethality should provide insight
127 into the functional importance of *Nv-Dnmt1a* for early embryonic development.
128 Therefore, we examined the embryonic development following *Nv-Dnmt1a*
129 pRNAi in more detail.

130 We first characterized the events of the first half of embryogenesis (0-15
131 hours, from egg lay to the completion of gastrulation) using time lapse imaging of
132 *Nv-Dnmt1a* pRNAi embryos. Similar to *D. melanogaster*, early development is
133 very rapid in *N. vitripennis.* During early embryogenesis, nuclei divide rapidly,
134 simultaneously, and without the formation of cell membranes to fill the large,
135 unicellular egg with syncytial nuclei. After 7 mitotic division cycles, nuclei migrate
136 to the cortex of the embryo, forming a syncytial blastoderm [41], consisting of a
137 single layer of nuclei populating the entire cortex of the egg. We observed no

138 obvious differences between control embryos and *Nv-Dnmt1a* pRNAi embryos
139 during the first 11 syncytial divisions. Syncytial blastoderm formation was
140 normal, and the last 4 divisions showed the characteristic increase in length
141 relative to earlier, pre blastoderm, cycles (Figure 1A).

142 The first obvious defect occurred at the 12th division cycle (Figure 1B, 1D).
143 There is normally a significant pause at this stage, as the nuclei are surrounded
144 by plasma membrane and thus transition from a syncytial to a cellular state, a
145 process referred to as cellularization (Figure 1A). Normally, cellularization
146 directly precedes the first morphogenetic movements of the embryo (gastrulation
147 and migration of the extraembryonic serosa) [41]. In this work, control embryos
148 began gastrulation 193 minutes after the onset of nuclear cycle 12, on average
149 (n=5, SD = 13.12, (Figure 1A)), similar to our previously published results in
150 untreated embryos [42]. Apparent morphogenetic movements in *Nv-Dnmt1a* pRNAi
151 embryos began significantly earlier, on average, 171 minutes (n=5, SD = 5.98)
152 into cycle 12 (Figure 1A).

153 In addition to being premature, these movements were abnormal. In *Nv-*
154 *Dnmt1a* pRNAi embryos, a line of cells at the anterior end of the embryo began
155 to ingress posteriorly (Figure 1D) which was not seen in control embryos (Figure
156 1B). In addition, internalization of the mesoderm and migration of the serosa from
157 the dorsal pole to cover the embryo both failed (Figure 1C, 1E).

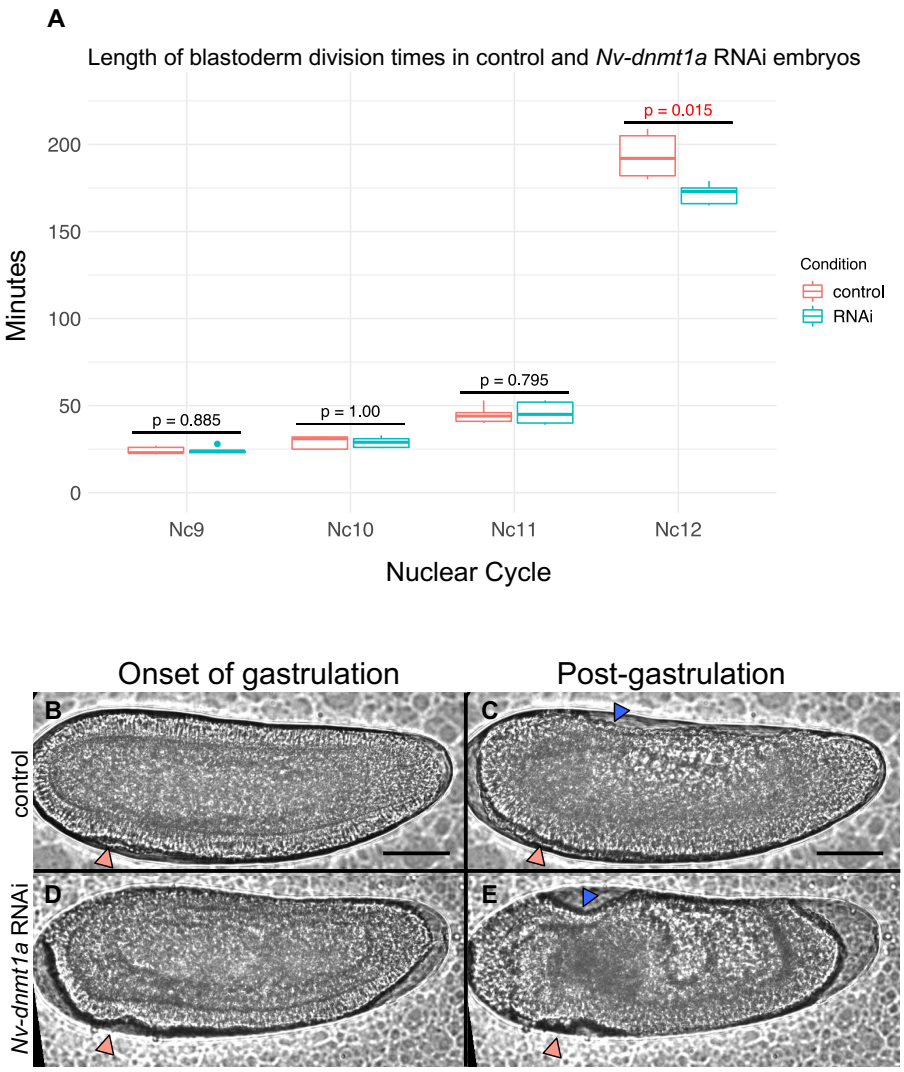

Figure 1. Analysis of time-lapse imaging of control and *Nv-Dnmt1a* RNAi embryos. **A:** Box and whisker plot displaying the length of blastoderm division times that were measured during live imaging experiments. Nc = nuclear cycle #. P values were determined by performing a 2-tailed t-test assuming unequal variance between RNAi and control. N=5 control, N=5 *Nv-Dnmt1a* RNAi. **B-C:** Still images from time-lapse of a control embryo at the onset of gastrulation (B) and at post-gastrulation. Peach arrow in (B) point to the initial mesodermal folds which are eventually internalized by post-gastrulation (C). The blue arrowhead in B indicates the serosa. **D-E:** Still images from time-lapse of an RNAi embryo at the onset of gastrulation and at the time equivalent to post-gastrulation. Defective mesodermal folds are denoted by peach arrowheads in D and E. Abnormal serosal movements are denoted by a blue arrowhead in E. Scale bars represent 50 µm.

173 To get a more detailed understanding of the cellular basis of these
174 defects, we examined high-resolution images of fixed and stained embryos at the
175 end of cycle 12 in control and knockdown samples. We imaged transverse
176 sections across the anterior-posterior axis of *Nv-Dnmt1a* pRNAi and control
177 embryos at the end of the 12th cell cycle, when the cellularization and the first
178 gastrulation movements should be occurring. Gastrulation in *N. vitripennis* is
179 different from what is seen in *D. melanogaster*. *N. vitripennis* embryos lack a
180 ventral furrow. Rather, the presumptive mesoderm on the ventral side of the
181 embryo forms a stiff plate. Subsequently, ectodermal cells separate from the
182 mesoderm at the lateral borders between the germ layers and crawl over this
183 mesodermal 'plate' before fusing over the mesoderm at the ventral midline [41].
184 During mid-cellularization, we observed membrane ingressing evenly
185 around each nucleus (Figure 2A) in control embryos. In contrast, membrane
186 ingression was uneven and did not wholly encapsulate nuclei in *Nv-Dnmt1a*
187 pRNAi embryos, leaving many nuclei completely or mostly uncovered prior to the
188 onset gastrulation (Figure 2C, white arrows point to examples of uncellularized
189 nuclei).
190 At the onset of morphogenesis, cell membranes fully enveloped each
191 blastoderm nucleus in control embryos, and a strong cable of actin was present
192 along the interior (basal) surface of the cellular blastoderm (Figure 2B-B', orange
193 arrowhead in 2B' marks the basal actin cable). Enlarged, round serosal cells
194 were present on the dorsal side, and the distinct population of presumptive
195 mesodermal cells was present on the ventral side (Figure 2C, pink arrowheads

196 mark the borders of the presumptive mesoderm), 24 out of 24 control embryos
197 are fully cellularized). In contrast, *Nv-Dnmt1a* pRNAi embryos lacked the cable
198 of actin along the interior surface of the blastoderm (Figure 2D-2D', orange
199 arrowhead marks uncellularized nuclei and obvious absence of the basal actin
200 cable), consistent with failed cellularization (23 out of 24 pRNAi embryos were
201 incompletely cellularized). In addition, the blastoderm was multilayered at many
202 locations, and clearly distinct serosal and mesodermal precursors were not
203 observed (Figure 2D).

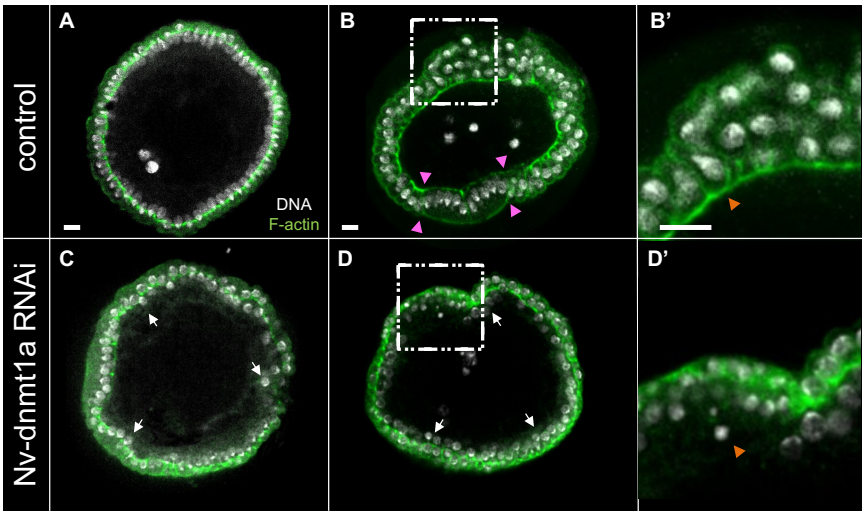

E

Condition	Cellularized	Incomplete Cellularization
Control	24	0
Nv-dnmt1a RNAi	1	23***

204

205 **Figure 2.** Transverse views of control and *Nv-Dnmt1a* RNAi embryos during
206 cellularization and at the onset of gastrulation. Green, phalloidin (F-actin). white,
207 DAPI (DNA). (A) Control embryo during mid cellularization. (B) Control embryo at
208 the onset of gastrulation. Pink arrowheads demarcate the borders of the
209 presumptive mesoderm. (B') Zoomed in view of fully cellularized control embryo.
210 Orange arrowhead points to the basal actin cable. (C) *Nv-Dnmt1a* RNAi embryo
211 during mid-cellularization. White arrows point to examples of disordered nuclei.
212 (D) *Nv-Dnmt1a* RNAi embryo at the onset of gastrulation. White arrows point to
213 examples of uncellularized, disordered nuclei. (D') Zoomed in view of an *Nv-*
214 *Dnmt1a* RNAi embryo that fails to fully cellularize. Orange arrowhead points to an

uncellularized nucleus (note the absence of the basal actin cable). (E) Table with n values of cellularized and incompletely cellularized control and *Nv-Dnmt1a* RNAi embryos. *** = p value < 0.0001 determined by Fisher's Exact Test. All scale bars (white lines in A-A''') represent 10 μm.

Nv-Dnmt1a is required for global gene body methylation

The failure of cellularization and morphogenesis are widely conserved indicators of disrupted MZT [42, 43, 44]. Consequently, we hypothesized that strong reduction of *Nv-Dnmt1a* by pRNAi would disrupt DNA methylation and dysregulate zygotic genome activation in the early embryo of *N. vitripennis*. We thus sought to characterize the DNA methylation patterns in the early embryo of *N. vitripennis* and to examine how this pattern was affected when *Nv-Dnmt1a* was depleted by pRNAi.

Sample	Non-conversion rate	Median CpG coverage	Mean CpG coverage	Methylated CpGs (mCGs)	mCGs within gene bodies
Control 1	0.0052	14	14.92	136,600	126,333
Control 2	0.0051	15	15.63	136,410	126,174
Control 3	0.0055	14	14.75	136,717	126,364
RNAi 1	0.0052	14	14.30	98,511	91,874
RNAi 2	0.0051	14	14.48	8,017	7,720
RNAi 3	0.0053	14	14.91	15,305	14,669

Table 1. Summary CpG statistics and non-conversion rates for each sample.

In control embryos (derived from mock-injected females) collected at the late blastoderm stage (7-9 hours after egg-lay, corresponding to the time where the developmental defects become evident) we identified 151,480 methylated CpGs (mCGs) in a union set representing all of the different mCGs across three

biological replicates. Each sample contained very similar numbers of mCGs across the three biological replicates (ranging from 136,410 to 136,717). The vast majority of these mCGs were found within gene bodies (Table 1).

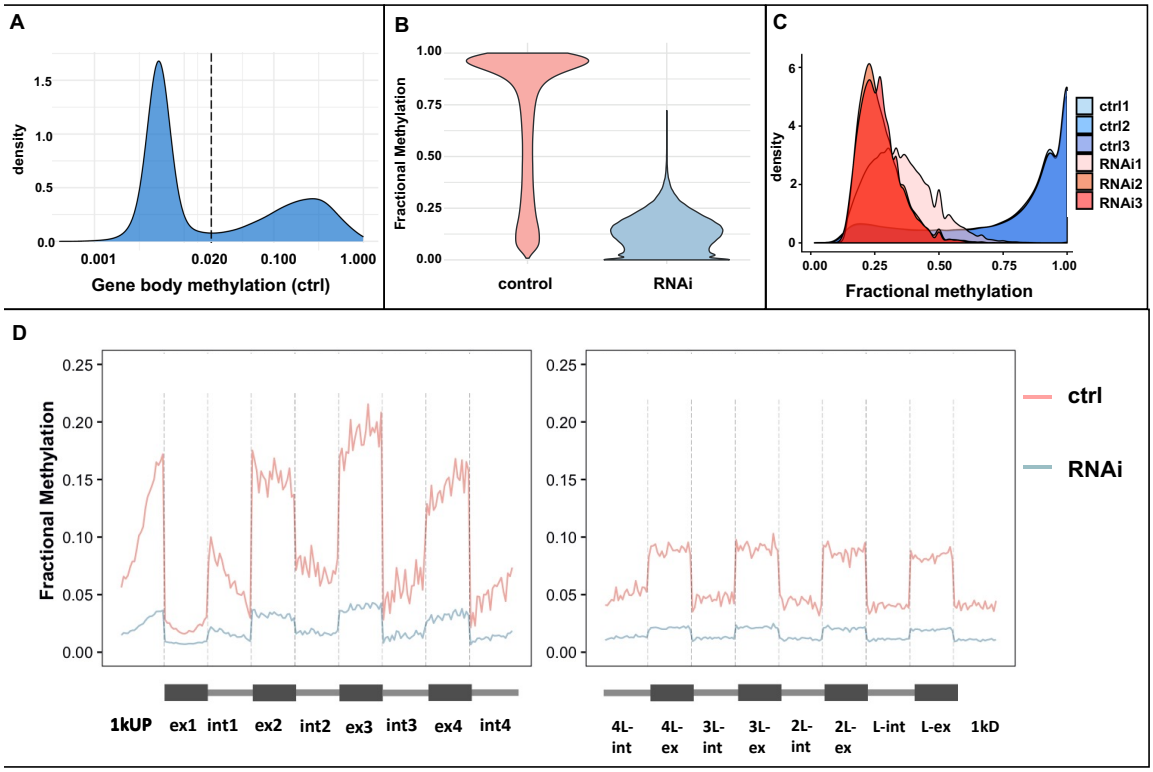

Figure 3. Global DNA methylation in control and *Nv-Dnmt1a* pRNAi late blastoderm *N. vitripennis* embryos. (A) An example of distribution of fractional DNA methylation in control embryo exhibiting the classical bimodal distribution. We defined methylated genes as genes with a minimum of 0.02 gene body methylation (shown as the dashed line) to classify methylated and unmethylated genes. (B) DNA methylation is substantially reduced in *Nv-Dnmt1a* pRNAi samples compared to the control samples. (C) Distributions of fractional methylation of CpGs that are methylated at least one control sample demonstrate that CpGs lose DNA methylation in RNAi embryos. (D) Distribution of mean fractional methylation in the first and last four exons and introns of methylated genes. Control samples shown in red, RNAi embryos shown in blue.

Mean fractional DNA methylation of gene bodies followed the canonical bimodal distribution (Figure 3A) as seen in other invertebrate species including

252 insects [27]. Following the criteria used in a previous study we designated genes
253 with gene body fractional methylation levels of at least 0.02 as methylated genes
254 [27]. By this criterion we found 5423 methylated genes in the blastoderm embryo.
255 This is fewer than the 6008 methylated genes identified in adult *N. vitripennis*
256 tissues [36], where a slightly different method to define methylated genes was
257 used. This difference was to some degree, but not entirely, due to the methods
258 used because when we used the method described in [36], the number of
259 methylated genes identified in our samples increased to 5,685. Regardless of the
260 methods, 99% of the genes we designated as "methylated" in the blastoderm
261 embryo were also identified as methylated genes in adult wasps [36]. This
262 indicates that our results are highly compatible with those of Wang et al., 2013 [36],
263 and are consistent with the idea that GBM patterns are generally stable across
264 life stages.

265 We knocked-down *Nv-Dnmt1a* mRNA levels with pRNAi and examined
266 DNA methylation at the same developmental stage (7-9 hours after egg lay) as
267 the control. Based on our RNAseq results, *Nv-Dnmt1a* mRNA levels were
268 reduced by 5-fold in late blastoderm pRNAi samples relative to late blastoderm
269 control samples [45]. We observed a significant reduction in DNA methylation at
270 99.7% of methylated CpGs in the genome in pRNAi embryos. The magnitude of
271 the reduction was substantial, as we found an average of 81.5% DNA
272 methylation depletion per mCG (Figure 3B, 3C and Table 1).

273 While DNA methylation was strongly reduced genome-wide, the intragenic
274 pattern of GBM was maintained. For example, mCGs were enriched in exons

275 and were more numerous at the 5' end of the coding region of gene bodies in
276 control embryos (Figure 3D) similar to patterns found in other insects and other
277 developmental stages [23, 35, 46]. This pattern was maintained in pRNAi embryos,
278 despite the drastic overall reduction in DNA methylation levels (Figure 3D). This
279 suggests that *Nv-Dnmt1a* is required for gene body methylation but does not
280 govern the 5' and exon-biased pattern of DNA methylation that we see in
281 *Nasonia* and other hymenopteran insects.

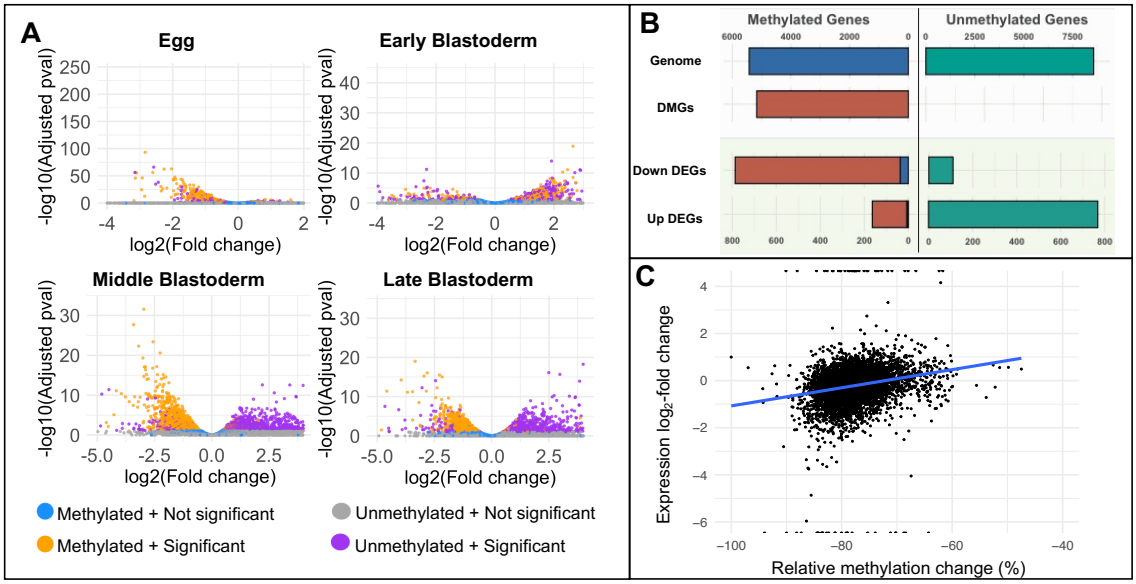

282

283 **Figure 4.** Gene expression of methylated and unmethylated genes in control and
284 *Nv-Dnmt1a* RNAi *N. vitripennis* embryos. **(**A) Volcano plots showing differentially
285 expressed genes between control and *Nv-Dnmt1a* RNAi in embryos of different
286 developmental stages. X axis is $\log_2$ fold change in *Nv-Dnmt1a* RNAi samples
287 relative to control samples. Y axis is $\log_{10}$ adjusted p-values. Golden dots are
288 methylated, significantly differentially expressed (FDR-corrected $P \leq 0.1$). Purple
289 dots are significant and DEGs that are unmethylated (FDR-corrected $P \leq 0.1$).
290 Blue and grey are non-significant and represent methylated and unmethylated
291 genes, respectively. (B) Distribution of methylated and unmethylated genes for all
292 genes in the genome, differentially methylated genes (DMGs), down-regulated
293 differentially expressed genes (Down DEGs), and up-regulated differentially
294 expressed genes (Up DEGs). (C) The correlation between relative GBM change
295 and relative expression change (calculated as $\log_2$-fold change) in the RNAi
296 samples compared to the control samples was positive and statistically
297 significant (Pearson R = 0.27, $P < 0.001$).

298 ***Loss of Nv-Dnmt1a function disrupts the regulation of a large proportion of***
299 ***the early embryonic transcriptome***

300 Given the profound effects of *Nv-Dnmt1a* on global DNA methylation and
301 early developmental events, we sought to understand the effects of *Nv-Dnmt1a*
302 knockdown on gene expression over time in the early embryo. Although the
303 developmental effects *Nv-Dnmt1a* pRNAi were not visible until cellularization and
304 the onset of morphogenesis, we hypothesized that changes in the transcriptome
305 in response to disrupted development would occur earlier in development,
306 leading up to the multifaceted failure of development at gastrulation.

307 To test this, we performed RNA-seq on timed egg collections from mock
308 injected (control) and *Nv-Dnmt1a* dsRNA injected wasps at time points that cover
309 early embryogenesis from egg laying to gastrulation. The collection time points
310 were: freshly laid eggs (0-2 hours after egg lay), early blastoderm (3-5 hours after
311 egg lay), middle blastoderm (5-7 hours after egg lay) and late blastoderm/onset
312 of gastrulation (7-9 hours after egg lay, when the corresponding WGBS data
313 were collected).

314 We observed that there is a massive increase in the number of genes
315 significantly affected by *Nv-Dnmt1a* pRNAi the middle blastoderm stage, and that
316 this increase is maintained into the late blastoderm (Fig 4A). We found 835 and
317 888 differentially expressed genes (DEGs) in the egg and early blastoderm
318 stages, respectively, while there were 2744 and 1831 DEGs in the middle and
319 late blastoderm stages, respectively. The middle blastoderm stage corresponds
320 to the most active part of the MZT, where maternal mRNAs are being finally

321 cleared and new transcription from the zygotic genome becomes the
322 predominant source of mRNAs.
323 Another intriguing pattern that appeared at the mid blastoderm stage is a
324 clear correlation between the direction of change of a DEG, and whether the
325 gene was methylated or not (unmethylated) at the late blastoderm stage (herein
326 referred to as 'mDEGs' for methylated DEGs, and 'uDEGs' for unmethylated
327 DEGs). Specifically, down-regulated transcripts in *Nv-Dnmt1a* pRNAi middle
328 blastoderm samples were largely derived from methylated genes (1201 out of
329 1331 (90%)), while upregulated transcripts mostly came from unmethylated
330 genes (1227/1413, 87%) (Figure 4A). Both of these observations were
331 statistically significant (Fisher's exact test, $P < 0.001$). A nearly identical pattern
332 was maintained into the late blastoderm stage (Fig. 4A, B).
333 Aside from the directions of change, we also observed that the
334 magnitudes of change at the gene level also differed between methylated and
335 unmethylated genes after *Nv-dnmt1a* pRNAi. For example, 93% (731/787) of
336 mDEGs at the late blastoderm stage were downregulated 4-fold or less, with a
337 significant proportion (315/787, 40%) being downregulated by less than two-fold
338 (Supplementary Figure 1A). The relative handful of up-regulated mDEGs showed
339 an even smaller magnitude of change, with 112/164 (68%) changing by 2 fold or
340 less (Supplementary Figure 1B). In contrast, uDEGs tended to show larger
341 magnitude changes, as 52% (323/619) of up-regulated uDEGs, and 35%
342 (39/110) of the down-regulated uDEGS changed by greater than 4-fold after
343 pRNAi relative to control (Supplementary Figure 1).

344 The strong over-representation of methylated genes in down-regulated
345 genes following *Nv-Dnmt1a* pRNAi fits well with previous observations in insects
346 connecting DNA methylation with increased and stable gene expression [19, 36, 47].
347 Furthermore, we have found that the magnitude of the reduction in expression
348 was highly correlated with the degree of lost methylation after pRNAi (Fig. 4C,
349 Pearson's correlation coefficient = 0.27, $P < 0.001$).
350 These observations imply that GBM plays an important role in maintaining
351 normal levels of high expression from methylated loci, and its loss leads to
352 widespread reduction in transcription from these loci. Assuming that GBM is the
353 sole molecular function of *Nv-Dnmt1a*, the effects on uDEGs, and potentially
354 some mDEGs, may be due to indirect effects downstream of the initial reduction
355 of mDEGs after pRNAi.
356 While indirect effects on unmethylated genes could be predicted, the very
357 strong bias toward upregulation of this gene class was quite surprising. We
358 compared our raw RNA-seq data and DESeq2 normalized data, to investigate if
359 any technical bias due to the normalization method could have affected our
360 inference of gene expression changes. There were no concerning or obvious
361 differences between the distribution of raw read counts and the normalized
362 counts used for our analyses (Supplementary Figure 2). Further the size-factors
363 required for normalization were all relatively small (Supplementary Table 1). This
364 indicates that there was no bias introduced by our normalization methods, and
365 that our results reflect a real signal in the transcriptome data.
366

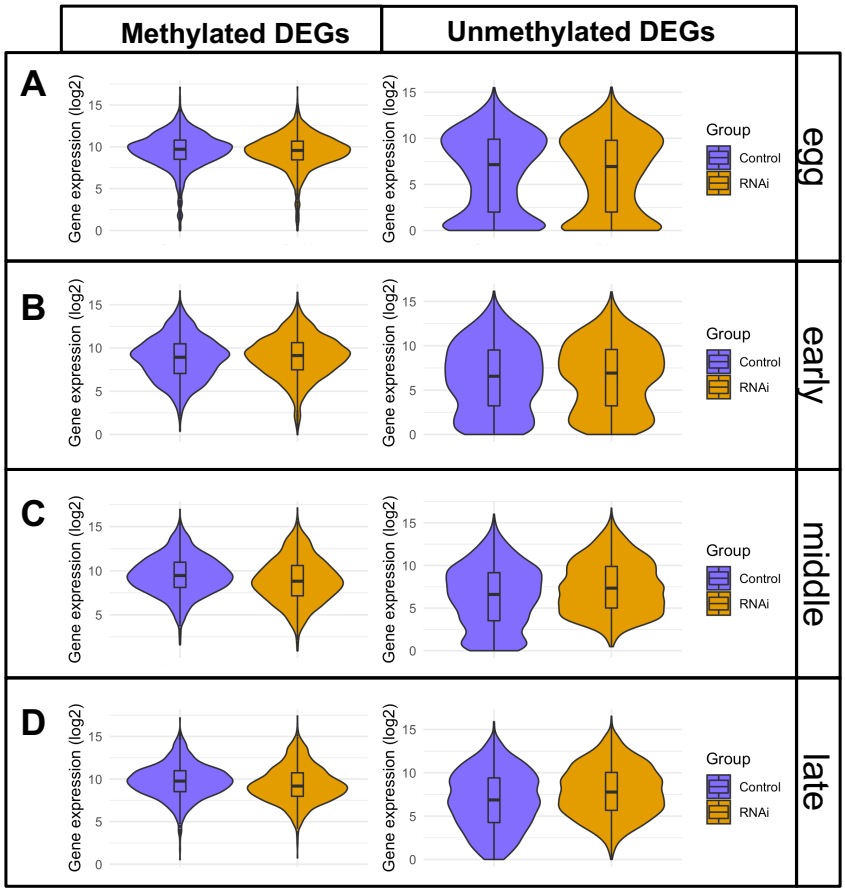

Figure 5. Violin plots of methylated and unmethylated differentially expressed genes (DEGs) in control and *Nv-Dnmt1a* pRNAi eggs, early blastoderm embryos, middle blastoderm embryos, and late blastoderm embryos.

Large-scale patterns of change differ between methylated and unmethylated differentially expressed genes

Due to the chaotic and variable nature of the failures of cellularization and morphogenesis, we hypothesized that the lethal phenotype is due to cascading effects initiated by direct effects of *Nv-Dnmt1a* pRNAi on methylated genes which could be amplified by the downstream effects on unmethylated genes. The strong correlation of DNA methylation state with the direction of expression level change (Figure 2C) is consistent with this hypothesis and indicates that there are

380 fundamental differences in how these classes of genes are regulated in the early
381 embryo. Thus, we further examined variation of gene expression among genes
382 that showed differential expression between control and *Nv-Dnmt1a* pRNAi
383 treatments in at least one stage (a total of 3904 genes).

384 We identified 1769 methylated differentially expressed genes (mDEGs),
385 which showed a remarkably stable pattern of expression across all stages,
386 consistent with our understanding of methylated genes in general [31, 36]. Most
387 mDEGs were clustered around the median and at relatively high expression
388 levels, with the frequency of higher and lower expressed genes tapering rapidly
389 and smoothly from this cluster. While the general shape of the distribution was
390 maintained after pRNAi, the average expression was shifted significantly
391 downward, particularly during the middle and late blastoderm stages (Figure 5).
392 When we isolated the relative handful of up-regulated mDEGs, we found that the
393 shape of the distribution shifted upward as expected, and also kept the same
394 shape with most genes clustered around the median expression level
395 (Supplementary Figure 3).

396 We identified 2135 unmethylated DEGs (uDEGs). In controls, uDEGs had
397 a low median expression level and there was no detectable enrichment in the
398 number of genes near this median level (Figure 5). Most noticeably, there was a
399 significant proportion of uDEGs that were expressed at very low levels, while
400 such low expression levels were almost absent in the mDEGs (Figure 5).

401 *Nv-Dnmt1a* pRNAi had little effect on global distribution of uDEG
402 expression levels in the egg and early blastoderm stages (Figure 5A, B),

403 consistent with the minor effects of pRNAi on these stages reported earlier
404 (Figure 4A). However, in the middle and late blastoderm stages (Figure 5C, D),
405 we observed that very few genes were expressed at the very low levels. This
406 indicates that uDEGs that were absent or expressed at very low levels in control
407 were present at significantly higher levels after *Nv-Dnmt1a* pRNAi. Similar, but
408 less pronounced patterns are observed when all genes, and non-DEGs are
409 plotted in similar way (Supplementary Figure 4).

410 Formally, there are two explanations for this pattern, which are not
411 mutually exclusive. Increased mRNA from a given gene could be due to excess
412 transcription from the locus. Alternatively, higher levels at a given time point
413 could be due to a disruption in degradation of mRNA from a previous stage,
414 leading to the presence of excess reads.

415 To identify potentially informative subsets of DEGs, that were not obvious
416 from the global comparisons above, we used hierarchical clustering to group
417 genes based on the similarity of their patterns of expression over time in control
418 embryos and maintained the order of genes in *Nv-Dnmt1a* pRNAi embryos to
419 facilitate direct comparisons. Gene expression levels at different time points and
420 treatments were then plotted according to these clusters (Figure 6A,B).

421 Among all the mDEGs identified across the four timepoints, we identified a
422 cluster of transcripts that show upregulation in the early blastoderm *Nv-Dnmt1a*
423 pRNAi embryos relative to control embryos (Fig. 6A, blue box, dotted lines). The
424 genes in this cluster were provided maternally at very high expression levels
425 (median log2 expression value of 10) in both control and pRNAi samples (Figure

426 6C). In control embryos, expression levels fell precipitously for these genes as

427 development progressed (median log2 expression value of 7, an 8-fold reduction

428 from control (Figure 6C)).

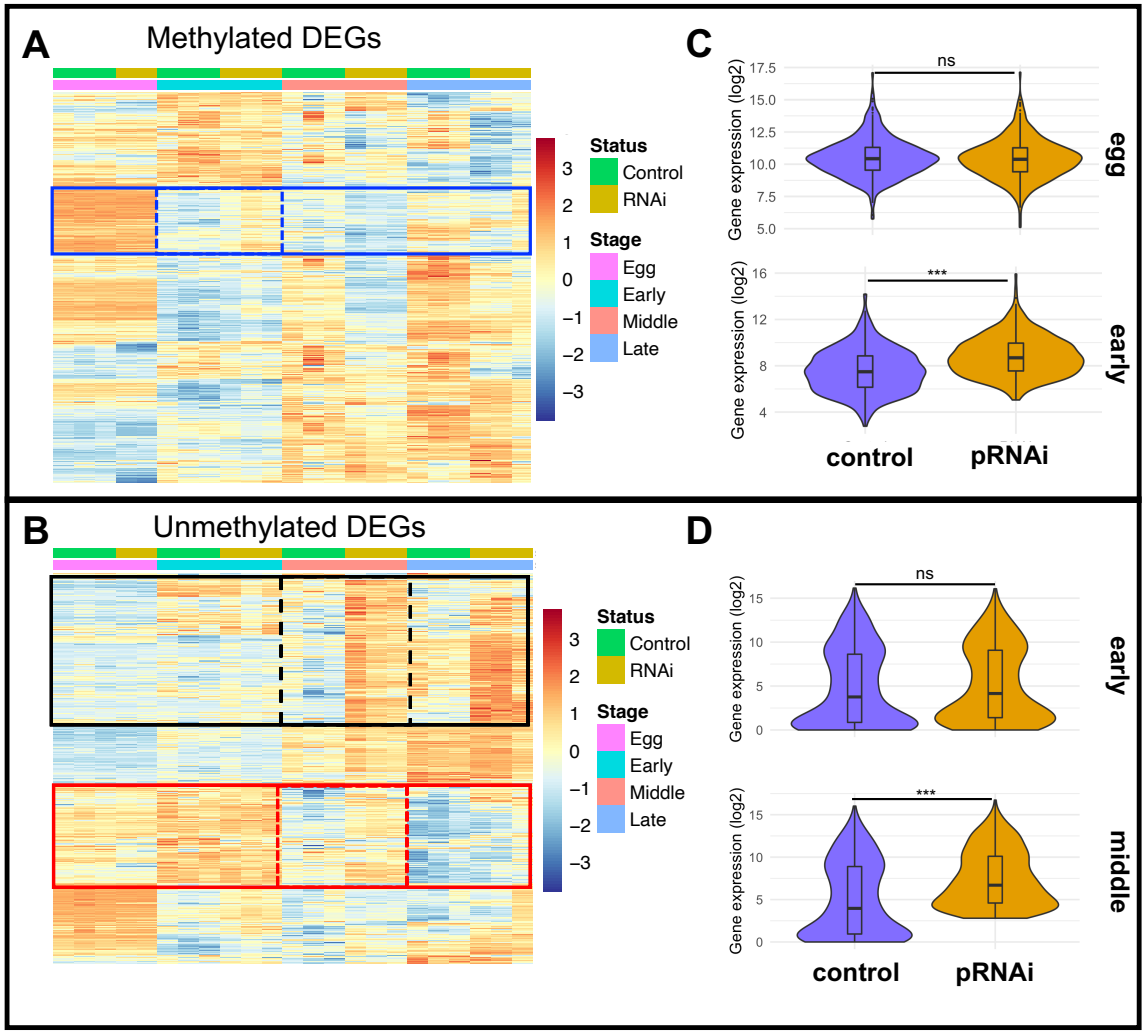

429

430 **Figure 6.** Differentially expressed methylated and unmethylated gene
431 expression in *Nv-Dnmt1a* pRNAi and control *N. vitripennis* embryos. (A)
432 Heatmap of 1769 methylated differentially expressed genes (mDEGs) and their
433 expression over time in control and *Nv-Dnmt1a* pRNAi samples represented as
434 Z-scores. Blue boxes on the heatmap highlight a cluster of mDEGs that are of
435 interest and discussed in the text. (B) Heatmap of 2135 unmethylated DEGs
436 (uDEGs) and their expression over time in control and *Nv-Dnmt1a* pRNAi
437 samples represented as Z-scores. Black and red boxes on the heatmap highlight
438 two clusters of uDEGs that are of interest and discussed in the text. (C) Violin
439 plots of 376 mDEGs in *Nv-Dnmt1a* pRNAi eggs and early blastoderm embryos.
440 These mDEGs are significantly enriched in the early blastoderm *Nv-Dnmt1a*

441 pRNAi samples relative to control early blastoderm embryos. Both comparisons
442 were subjected to a t-test. ns = not significant, *** P<0.001 by t-test.
443 (D) Violin plots of 213 uDEGs in control and *Nv-Dnmt1a* pRNAi early and middle
444 blastoderm embryos (B). ns = not significant, *** P<0.001 by t-test.
445
446

447 In *Nv-Dnmt1a* pRNAi embryos, the levels of this set of genes also fall
448 significantly from egg to early embryo, but the magnitude of reduction is smaller
449 (median log2 expression value of ~8, a 4-fold reduction in median level), leading
450 to the appearance of upregulation relative to control at this stage (Figure 6C).
451 Thus, it appears that mRNA degradation downstream of Nv-Dnmt1a function
452 plays an important role in regulating levels maternally expressed, methylated
453 genes.

454 Among the uDEGs, we identified two clusters of interest. The larger of
455 these (Figure 6B, see black box) show much higher expression in middle and
456 late blastoderm in *Nv-Dnmt1a* pRNAi embryos relative to control. Expression
457 levels of these uDEGs are at low to moderate levels in eggs and early
458 blastoderm embryos in both control and pRNAi and remain so in the later stages
459 of control embryos (Figure 6B, compare consistent "cool" colors as opposed to
460 increased warmth in the RNAi samples). When we plot genes corresponding to
461 this cluster (change less than 2-fold between early and middle blastoderm
462 control, and are significantly higher after pRNAi in the middle blastoderm), we
463 found that 437 genes are mostly expressed at very low levels in the early
464 blastoderm in both control and pRNAi. At the middle blastoderm stage, there is a
465 significant general increase of these genes in the pRNAi case, while they remain
466 mostly unchanged at low levels in the control (Figure 6D). The most likely

467 explanation for this pattern is that the increased levels in pRNAi embryos are due
468 to improper activation of these genes at the middle and late blastoderm stage.
469 There is another cluster of uDEGs whose relative levels in control
470 embryos increase markedly in the early blastoderm stage and then fall steeply in
471 the subsequent stages (Figure 6B, see red box). In *Nv-Dnmt1a* pRNAi embryos,
472 the initial increase is not affected, but levels do not fall as significantly at later
473 stages, leading to an apparent upregulation of their transcripts relative to control
474 embryos in later stages (Figure 6B). The 615 genes that fit this profile show
475 again very similar distributions between the control and pRNAi cases in the early
476 blastoderm. In contrast there is a severe drop in levels for the control embryos at
477 the middle blastoderm stage, while the pRNAi levels decrease less dramatically
478 (Supplementary figure 5). This pattern is similar for the 376 mDEGs that were
479 apparently upregulated in the early blastoderm stage (Figure 6A,C) and indicates
480 that regulation of mRNA degradation is affected downstream of *Nv-Dnmt1a*
481 pRNAi during the major phase of the MZT.
482
483 ***Many potential targets for mediating the developmental effects of Nv-***
484 ***Dnmt1a pRNAi***
485 While there is no single obvious candidate gene to explain our results,
486 there are many RNA binding and regulating factors, as well as transcription
487 factors, cyclins and cytoskeletal components that could plausibly play important
488 roles in producing the patterns of gene expression change and developmental
489 failure after pRNAi. We performed gene ontology analyses, and found that terms

490 involved in metabolism, and other basal cell functions were the most significantly
491 and consistently enriched in both in methylated and unmethylated DEGs
492 throughout development (Supplementary Table 2). In addition, we found that
493 RNA degradation is an enriched category of methylated genes, which could
494 explain part of the pattern of gene expression change (Supplementary Table 2).
495 Among the RNA binding factors affected by *Nv-Dnmt1a* pRNAi are
496 homologs of the well-known MZT factors *Smaug* and the CCR-NOT deadenlyase
497 complex. Fascinatingly, we also found that an ortholog of the *D. melanogaster*
498 nonsense mediated mRNA decay (NMD) component *nonC (Nv-nonC)* was down-
499 regulated after *Nv-Dnmt1a* pRNAi. While the *D. melanogaster* gene has no role
500 in embryogenesis [48], the mouse ortholog (named Smg1 after the *C. elegans*
501 gene (no relation to *smaug*), which is the founding member of this gene family [49])
502 is required for embryogenesis [50]. Furthermore, the human ortholog of
503 *Smg1*/*nonC* is regulated by DNA methylation in humans [51]. We decided to
504 functionally test whether *Nv-nonC* could be an important intermediary in
505 producing the defects in cellularization and gastrulation when *Nv-Dnmt1a* was
506 knocked down.
507 Live imaging of *Nv-nonC* knock-down embryos revealed that affected
508 embryos consistently arrested at nuclear cycle 11 and did not proceed to the final
509 syncytial division or gastrulation (compare Supplementary Movie 1 (control) to
510 Supplementary Movie 2 (*Nv-nonC* RNAi)). This is more severe than the strongest
511 *Nv-Dnmt1a* phenotypes, so we cannot say for certain the exact role of *Nv-nonC*
512 in the regulatory networks downstream of *Nv-Dnmt1a* at the moment. However,

513 the phenotype is consistent with *Nv-Smg1* having an important role in the
514 transition from egg to embryo, and its partial reduction and disturbance of its
515 potential interaction partners after *Nv-Dnmt1a* pRNAi might play a significant role
516 in the failures of cellularization and gastrulation.
517
518 **Discussion**
519 A previous study found that one of the DNMT1 orthologs in the wasp (*Nv-*
520 *Dnmt1a*) was required for *Nasonia* embryogenesis, while the other two DNMT1
521 paralogs (*Nv-Dnmt1b*, *Nv-Dnmt1c*) and the DNMT3 ortholog *Nv-dnmt3* were
522 apparently dispensable [39]. *Nv-Dnmt1a* pRNAi embryos failed to form segments
523 and the knockdown was lethal [39] which led us to further examine the phenotype
524 in more detail [52, 53].
525 We found that the first signs of developmental failure are nuclei that fail to
526 be correctly cellularized. This directly precedes failure of the morphogenetic
527 processes of mesoderm internalization, and migration of the serosa. These are
528 all developmental events that are strongly affected when the MZT is disrupted in
529 *N. vitripennis* and *D. melanogaster*. Consistent with this, *Nv-Dnmt1a* knockdown
530 was associated with major disruption of gene expression levels during early
531 embryogenesis. The most significant alterations to the transcriptome occurred at
532 the mid blastoderm stage, which correlates well with when the major wave of
533 zygotic genome activation occurs in *N. vitripennis*. This observation, in
534 combination with our finding that GBM was significantly reduced after *Nv-Dnmt1a*

535 pRNAi, strongly indicates that loss of gene body methylation disrupts the MZT in
536 *N. vitripennis*.
537 The exact mechanism by which Nv-Dnmt1a regulates the MZT and
538 downstream processes is not yet understood. However, our current results
539 provide a good basis to generate hypotheses. A crucial observation was that
540 there was an extremely strong correlation between methylation state of a gene
541 and the direction of expression change after *Nv-Dnmt1a* pRNAi: downregulated
542 genes in pRNAi embryos were almost all methylated in control embryos, and
543 upregulated genes were conversely almost exclusively unmethylated (Figure 4).
544 Previous studies posited that gene body methylation has an important role
545 in facilitating high, steady levels of gene expression [17, 36]. However, whether gene
546 body methylation directly regulates levels of gene expression has been
547 controversial [54, 55]. Phylogenetic analyses of methylated and unmethylated plant
548 species as well as analyses of within-species variation of gene body methylation
549 in plants [54, 55, 56] led to at most weak effects of gene body methylation on gene
550 expression, although the evolutionary conservation of gene body methylation
551 indicated associated functionality. Here we show that as a result of pRNAi of *Nv-*
552 *Dnmt1a*, the vast majority of methylated genes that are differentially expressed
553 show reduction of gene expression. Moreover, the degree of expression
554 reduction directly correlated with the degree of gene body methylation loss. As
555 far as we are aware, these are the first such demonstrations directly linking gene
556 body DNA methylation to gene expression levels.

557 Another novel finding is that a large proportion of the unmethylated
558 differentially expressed genes were upregulated in *Nv-Dnmt1a* pRNAi relative to
559 control. Presumably the effects of *Nv-Dnmt1a* pRNAi on unmethylated genes are
560 indirect and are more proximally caused by the disrupted expression of the
561 methylated genes. It is not clear why such indirect effects result in such a large
562 bias toward increased gene expression. However, we noticed that the bulk of
563 unmethylated genes cluster at very low expression levels in the blastoderm
564 stages (Figure 5), and that most of the change in unmethylated genes we
565 observe after *Nv-dnmt1a* knockdown is a subset of these lowly expressed genes
566 being significantly increased (Figure 5). We propose that one or more mDEG is
567 important for keeping the lowly expressed transcripts at low levels (by either
568 repressing transcription or encouraging transcript degradation). Future
569 experiments will employ techniques that can specifically detect changes in
570 mRNA regulation and transcription initiation to determine how these processes
571 affect indirect targets of Nv-Dnmt1a and potentially which direct targets mediate
572 these effects.
573
574 The roles of DNMT1 orthologs in methylation and development have been
575 explored in other insects. In the cockroach, *Blatella germanica*, *Dnmt1* RNAi
576 results in embryonic lethality visible both before and after gastrulation [19]. The
577 effects of disrupting the MZT are less well understood in hemimetabolous
578 insects, but strong *B. germanica zelda (BgZelda)* RNAi knockdown leads to early
579 embryonic lethality similar to that of *B. germanica Dnmt1* (*BgDnmt1*) [57].

580 BgDnmt1 RNA leads to reduced GBM, and significant changes in both
581 methylated and unmethylated genes. However, both sets of genes show equal
582 amounts of up- and down-regulation, which is in contrast to what we see at the
583 middle and late blastoderm stages [19]. This could simply be due to changes the
584 role of GBM and the regulatory networks downstream of methylated genes that
585 have accumulated since the wasp and roach lineages diverged. Alternatively,
586 while our samples were precisely focused on capturing events directly at the
587 MZT, the samples examined in *B. germanica* were necessarily less temporally
588 restricted and extended further in developmental time. This may have allowed
589 for downstream knock-on effects to overwhelm a potentially conserved signal of
590 increased uDEGs and decreased mDEGs at the critical point in the MZT. More
591 studies of Dnmt function with a focus on the events of the MZT in other insects
592 will be required to resolve these questions.
593 Results of *Dnmt1* knockdown in the milkweed bug *Oncopeltus fasciatus*
594 and the beetle *Tribolium castaneum* indicate that Dnmt proteins may have
595 important functions not related to their methylation function [35, 58, 59]. In *O.*
596 *fasciatus*, GBM methylation was shown to be dependent on its Dnmt ortholog in
597 adults, and pRNAi against it led to disruption of oogenesis. However, no
598 significant changes in gene expression were detected in ovaries, or in other adult
599 tissues, raising the question of whether GBM is functionally relevant for
600 oogenesis [35]. Subsequently, *O. fasciatus* Dnmt was shown to be crucial for
601 meiosis in male testis, but again in and apparently GBM independent manner [58].
602 Consistent with this, *T. castaneum* still retains a Dnmt1 ortholog (but lacks

603 Dnmt3), but shows no significant genomic cytosine methylation [59]. Despite this,
604 knockdown of *T. castaneum* Dnmt1 leads to early embryonic lethality, indicating
605 methylation independent functions for Dnmt1 orthologs in beetles and bugs.
606 We believe that the clear correlation between reduction of methylation and
607 reduction of expression level of methylated genes is strong evidence that the
608 methyltransferase function of Nv-Dnmt1a is the major reason *Nv-Dnmt1a* is an
609 essential gene in *N. vitripennis*. However, we certainly cannot exclude that
610 additional functions of the protein exist, and that they contribute to the complex
611 phenotypes we observed after knocking down *Nv-Dnmt1a* with pRNAi. A
612 significant portion of our future aims is to isolate the role of GBM from other
613 potential effects of the RNAi. We also look forward to studies in other insects
614 that will show whether additional functions of Dnmt1 orthologs are novel,
615 ancestral or some combination of both.
616
617 Finally, our results point to the middle blastoderm stage as the crucial
618 point where *Nv-Dnmt1a* has its strongest effects on the embryonic transcriptome.
619 Our data also show that the indirect effects of *Nv-Dnmt1a* pRNAi are mediated
620 by both disruption of mRNA degradation, and misregulation of transcription from
621 the zygotic genome. Thus, *Nv-Dnmt1a* appears to exert its strongest effects at
622 the time, and using the molecular processes, that are most characteristic of the
623 MZT. We therefore propose that GBM is a crucial component of the MZT in
624 *Nasonia*, and that this epigenetic mark is likely to play an important role in the
625 MZT in other insects.

626

627 **Acknowledgements**

628 We thank The University of Chicago Genomics Facility (RRID:SCR_019196), for

629 their very valuable assistance with generating the WGBS and RNAseq data.

630 This work was supported by grant MCB1615664 from NSF to SVY, and by grants

631 R01GM129153 and R03HD087476 from NIH to JAL.

632

633 **Methods**

634 Live imaging

635 All embryos were live-imaged as described in Arsala & Lynch 2017 [42]. Briefly, we

636 live-imaged all embryos at 28C for 15 hours on an Olympus BX-80 inverted

637 microscope under 30X silicone immersion and DIC optics.

638

639 Embryo Collection

640 All embryos used for fluorescence in situ hybridizations were collected and fixed

641 as described as in Buchta et al., 2013 [41].

642

643 Ovary Collection

644 Mothers were cold anesthetized and their ovaries were hand-dissected and

645 extracted using stainless-steel needles. The ovaries were fixed in 5%

646 formaldehyde for 30 minutes and subsequently used for fluorescence in-situ

647 hybridization.

648

649 Phalloidin staining & transverse sectioning

650 Control injected and *Nv-Dnmt1a* dsRNA (1ug/ul) injected mothers were allowed
651 to lay eggs on hosts for 2 hours at 25C. Freshly laid eggs were collected from
652 hosts and aged on 1% agarose PBS plates at 25C until they were 8-10 hours old,
653 so that all embryos were aged to correspond with the onset of gastrulation. We
654 hand dissected the chorions of fixed embryos. Afterward, the fixed embryos
655 were placed in 1X PBS and stained with AlexaFluor 488 phalloidin at a 1:250
656 dilution. The stained, fixed embryos were placed in vectashield with DAPI
657 overnight. Finally, the embryos were laid flat on a cover slip and were cut in half
658 along the transverse axis using a razor slotted into an embryo 'guillotine.' The
659 resulting embryo 'halves' were flipped 'up' on the cover slip and imaged on an
660 Andor Revolution WD spinning disc confocal system. The samples were
661 illuminated with 488nm (phalloidin) and 405nm (DAPI) diode laser and Z-stack
662 images were captured using a 30x objective at 1micron increments.

663

664 RNA extraction

665 Embryos were collected and aged as described above. We designed 3 non-
666 overlapping dsRNA constructs and injected 100 females per biological replicate
667 with either 1µg/mL dsRNA diluted in water or with water as a control. The
668 females were left unmated, so that all resulting progeny were male as the
669 variation in sex and ploidy could confound our analysis. The injected females
670 were allowed to lay eggs that were aged at 25C until they reached the following
671 four time points across the MZT: 0-2hours to generate a freshly laid egg

672 transcriptome, 3-5hours to generate an early blastoderm transcriptome, 5-7
673 hours to generate a middle blastoderm transcriptome, 7-9 hours to generate late
674 blastoderm embryos that are at the onset of gastrulation. Once the embryos
675 reached the time points, we isolated 100ng of total RNA using TRI Reagent for
676 all samples in biological triplicate. We confirmed the RIN value for all samples
677 were above 9.0 using a 2100 Agilent Bioanalyzer and immediately prepared 24
678 libraries for sequencing.
679
680 RNA library preparation and bulk RNA-sequencing
681 Using the 100ng of total RNA from each sample isolated above, we performed
682 poly-A tail selection using the NEBNext Poly (A) mRNA magnetic isolation
683 module (E7490) and immediately proceeded with library preparation. Libraries
684 were prepared for bulk RNA-sequencing using the NEBNext Ultra Directional
685 RNA Library Prep Kit for Illumina (E7420). The libraries were purified, validated
686 and pooled before sequencing. The libraries were subjected to 100bp paired-end
687 sequencing across 2 lanes on a HiSeq4000. Raw data from this analysis can be
688 found in the NCBI BioProject archive with accession number PRJNA701367.
689
690 RNA-seq analysis
691 To assess sequencing quality, we using FastQC and saw high quality reads
692 across all samples. We trimmed adapters and removed low quality reads using
693 Trim Galore-0.6.0 only using the --paired parameter. We reassessed the trimmed
694 read quality using FastQC and proceeded to map the reads to genome using

695 HISAT2-2.0.5 (hisat2 -p 8 --max-intronlen 10000 -q –x). Differential expression
696 analysis was performed using the R package DESeq2[60].
697
698 DNA extraction and bisulfite library preparation
699 We extracted and purified genomic DNA from embryos using the QIAamp DNA
700 Micro Kit (Qiagen 56304). 40ng of genomic DNA was bisulfite converted and
701 libraries were prepared at the University of Chicago Genomics Facility using the
702 Accel-NGS Methyl-Seq DNA Library Kit from Swift Biosciences. Raw bisulfite
703 sequencing reads can be found in the NCBI BioProject archive with accession
704 number PRJNA701143.
705
706 Analysis of Bisulfite-sequencing data
707 CpG sites were determined to methylated using a binomial test [22, 36] where the
708 rate of deamination representing the probability of success and total number of
709 reads representing the number of trials [22, 36]. P-values were then corrected for
710 multiple testing [61] and CpGs with adjusted P-values of < 0.05 were labeled as
711 methylated CpGs. Genes containing at least one methylated CpG were
712 subsequently labeled as methylated genes. Fractional methylation of CpGs was
713 calculated by dividing the number of methylated reads by the total number of
714 reads and the fractional methylation of genes was calculated by taking the
715 average fractional methylation of all CpGs within the gene body.
716 For the differential methylation analysis, only CpG sites that were methylated in
717 at least one control sample were retained similar to previous insect studies [47, 62].

718 The DSS package [63] was used to assess differentially methylated CpGs with
719 RNAi status as the sole predictor of methylation. P-values for each CpG site was
720 adjusted for multiple testing [61] with significance level set at an adjusted P-value
721 of < 0.1. Genes with at least one differentially methylated CpG were considered
722 as differentially methylated genes.
723

724 **Supplementary Data:**

Sample	Size Factor
Egg control rep 1	2.008
Egg control rep 2	2.618
Egg control rep 3	2.389
Egg RNAi rep 2	1.855
Egg RNAi rep 3	2.422
Early control rep 1	0.799
Early control rep 2	0.789
Early control rep 3	1.041
Early RNAi rep 1	0.945
Early RNAi rep 2	1.234
Early RNAi rep 3	1.004
Middle control rep 2	0.848
Middle control rep 3	0.609
Middle RNAi rep 1	0.709
Middle RNAi rep 2	0.835
Middle RNAi rep 3	0.843
Late control rep 1	0.763
Late control rep 2	0.891
Late control rep 3	0.689
Late RNAi rep 1	0.822
Late RNAi rep 2	0.461
Late RNAi rep 3	1.026

725

726 **Supplementary Table 1.** Size Factors used for normalization of RNAseq
727 libraries
728

729

Category	Enriched terms	Count	%	P-Value	Benjamini
KEGG_PATHWAY	RNA degradation	16	2.1	0.00018	0.014
KEGG_PATHWAY	Oxidative phosphorylation	28	2.4	0.00064	0.032
KEGG_PATHWAY	Proteasome	16	1.4	0.00061	0.059
KEGG_PATHWAY	Basal transcription factors	10	1.3	0.0032	0.083
KEGG_PATHWAY	Endocytosis	21	2.7	0.0016	0.063
COG_ONTOLOGY	Translation, ribosomal structure and biogenesis	10	1.3	0.0023	0.044

Supplementary Table 2. GO Analysis for down-regulated methylated genes in middle and late blastoderm *Nv-Dnmt1a* RNAi embryos

Gene	Forward Primer	Reverse Primer
Nv-dnmt1a	ggccgcggAGCGTCGATGCCTACTTATG	cccggggcAGCTTGTTCTCCACCATCAA
Nv-dnmt1a	ggccgcggACGTATGACTGGGTTGAGTC	cccggggcGGAGCATGAAGTTGGAACAC
Nv-dnmt1a	ggccgcggttaatcactacccccctgcat	cccggggcatgtttcgcccaatactgtt
Nv-nonC	GGCCGCGGCCTTGAGAAACGGACAGAGA	CCCGGGGCGAAGACATTGGCTCGGTTTC

Supplementary Table 3. Primers names and sequences

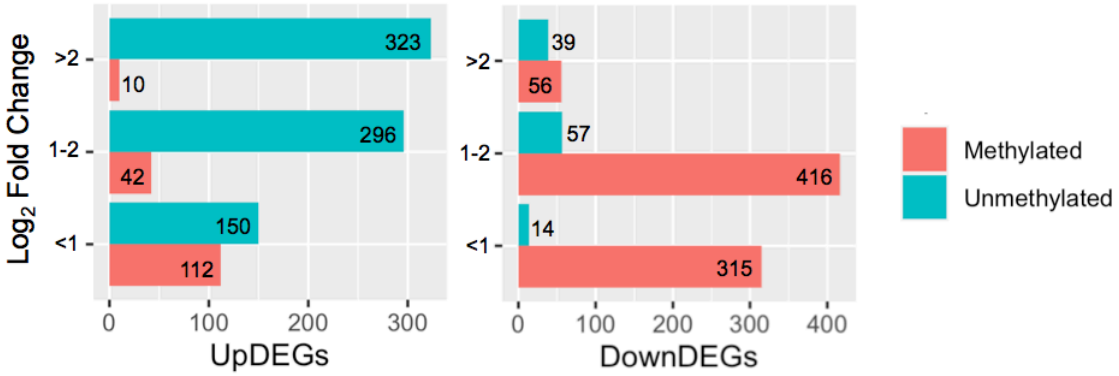

Supplementary Figure 1. Bar graphs showing the number of upregulated differentially expressed genes (UpDEGs) and downregulated differentially expressed genes (DownDEGs).

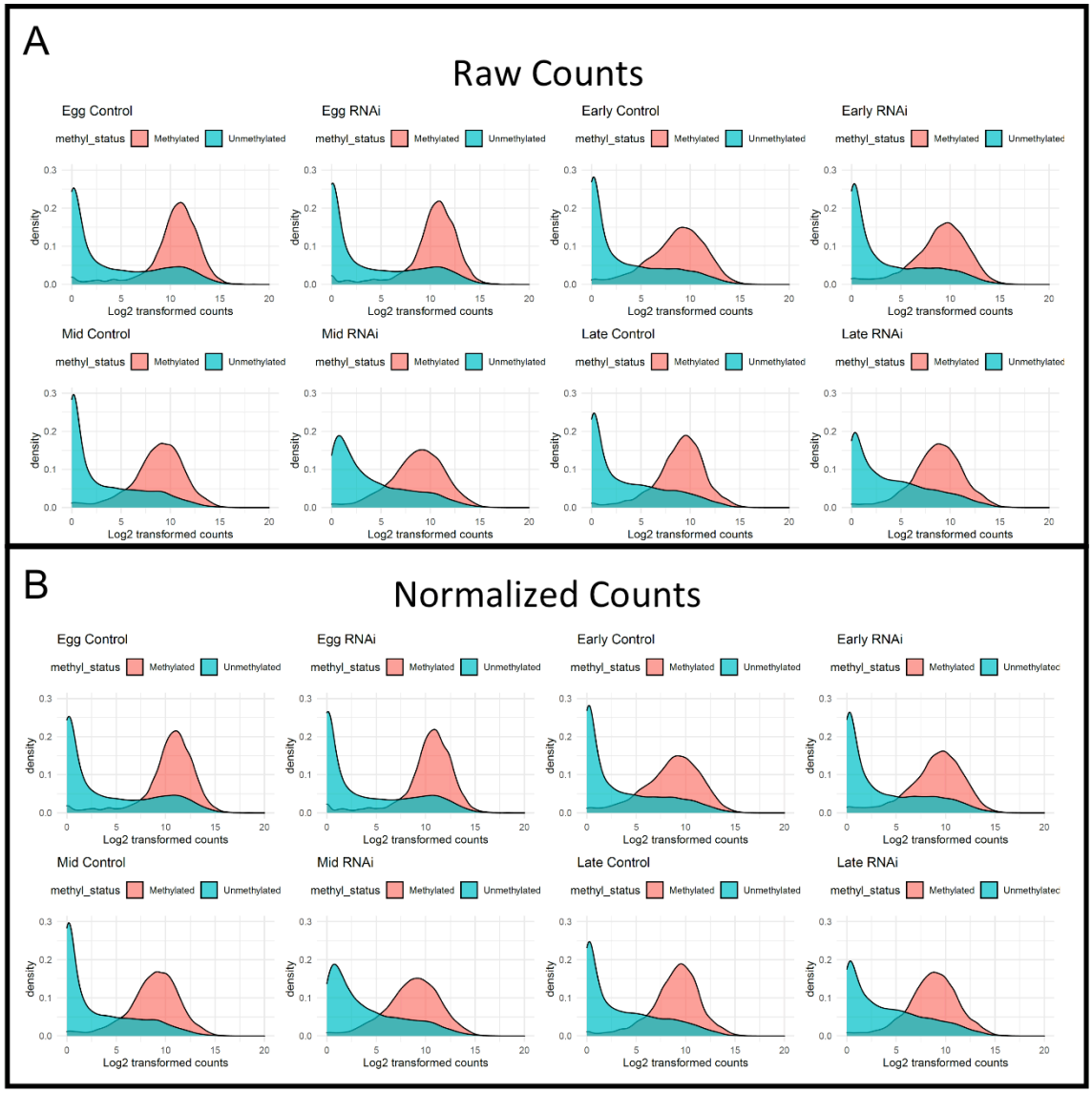

Supplementary Figure 2. Density distributions of (A) raw transcriptome read counts and (B) normalized counts from DESeq2. Data are log2-transformed. Methylated and unmethylated genes exhibit distinctive patterns of expression consistent with previous studies. The density distributions of the raw and normalized counts are highly similar.

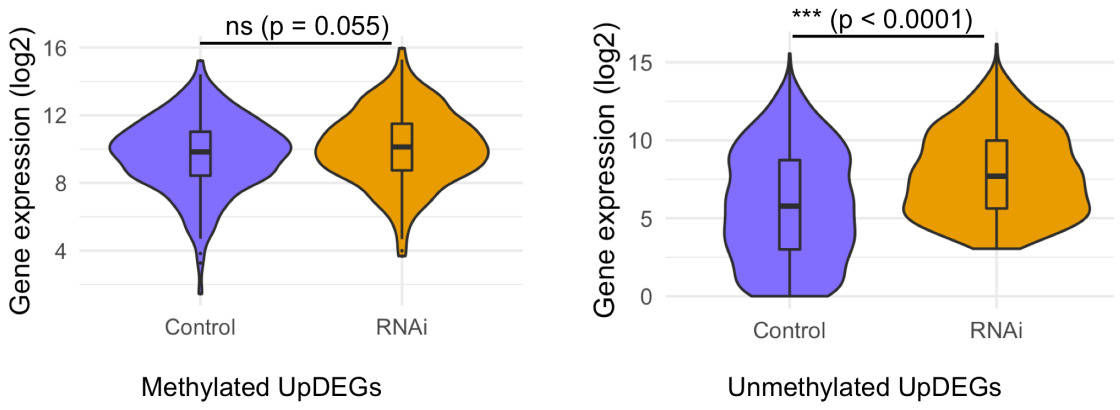

Supplementary Figure 3. Violin plots of methylated and unmethylated upregulated differentially expressed genes during the late blastoderm stage in control and *Nv-dnmt1a* pRNAi embryos.

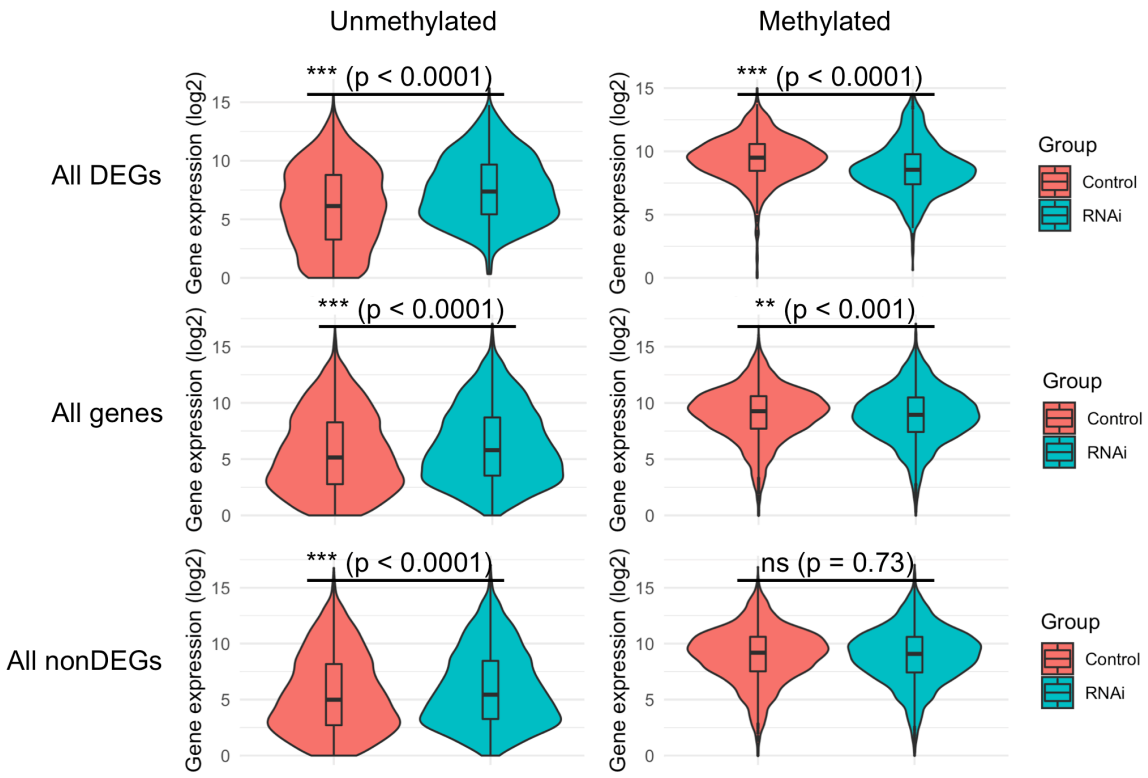

Supplementary Figure 4. Violin plots of methylated and unmethylated genes during the late blastoderm stage in control and *Nv-dnmt1a* pRNAi embryos broken up into three categories: top, all differentially expressed genes (All

764 DEGs), middle, all genes, and bottom, all non-differentially expressed genes (All
765 nonDEGs).
766
767
768

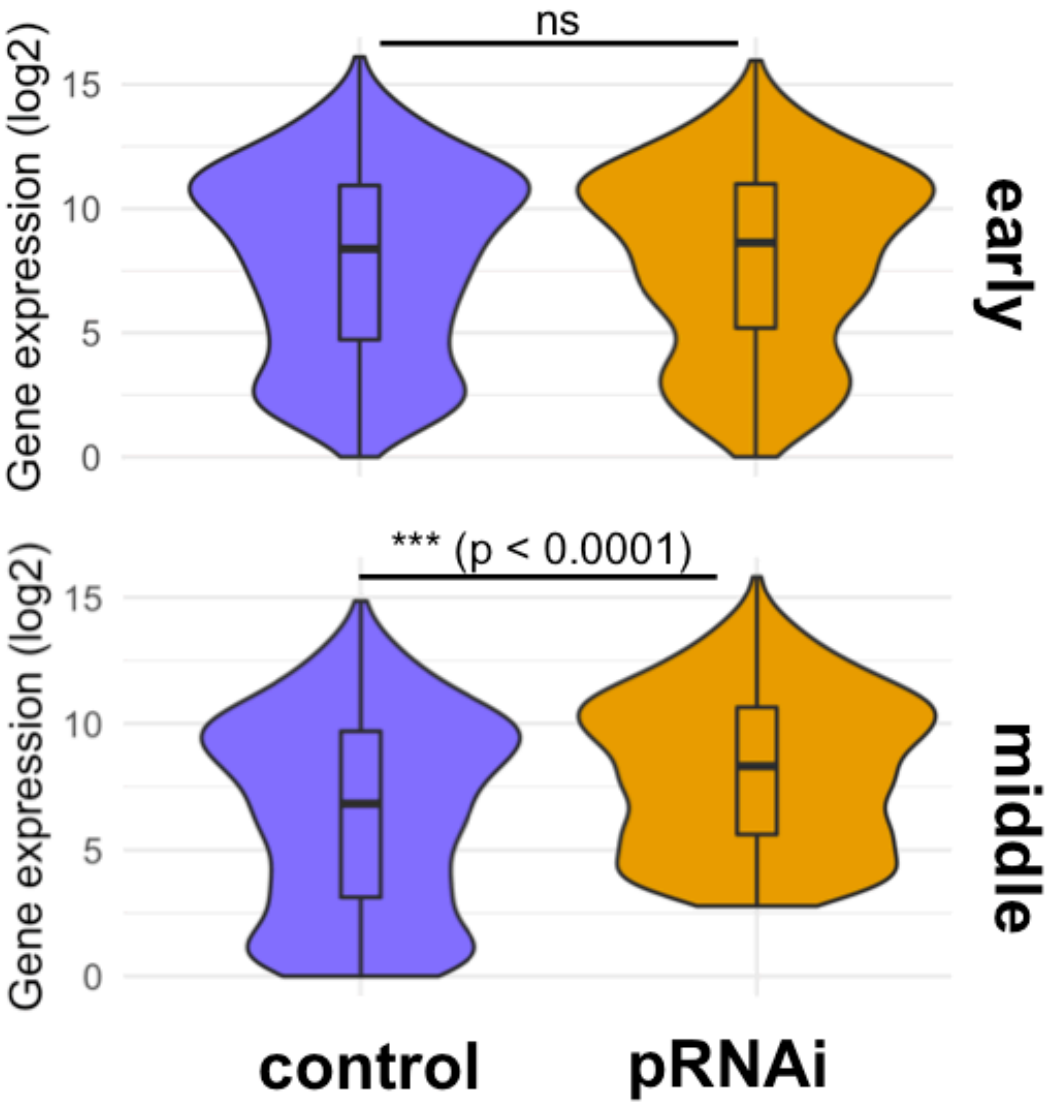

769
770 **Supplementary Figure 5.** Violin plots of 615 genes that have a similar
771 expression profile between control and *Nv-dnmt1a* pRNAi early blastoderm
772 embryos and a significant difference in their expression in between control and
773 pRNAi middle blastoderm embryos.
774
775
776
777 **Supplementary Movie 1.** Time lapse movie of developing control, mock-
778 injected, embryo. 1 image taken per minute. Anterior is to left.

Supplementary Movie 2. Time lapse movie of developing *Nv-nonC* knockdown embryo. 1 image taken per minute. Anterior is to left.

References

1. Tadros W, Lipshitz HD. The maternal-to-zygotic transition: a play in two acts. *Development* **136**, 3033-3042 (2009).

2. Vastenhouw NL, Cao WX, Lipshitz HD. The maternal-to-zygotic transition revisited. *Development* **146**, dev161471 (2019).

3. Tadros W*, et al.* SMAUG is a major regulator of maternal mRNA destabilization in Drosophila and its translation is activated by the PAN GU kinase. *Developmental cell* **12**, 143-155 (2007).

4. Laver JD*, et al.* Brain tumor is a sequence-specific RNA-binding protein that directs maternal mRNA clearance during the Drosophila maternal-to-zygotic transition. *Genome biology* **16**, 94 (2015).

5. Fu S, Nien C-Y, Liang H-L, Rushlow C. Co-activation of microRNAs by Zelda is essential for early Drosophila development. *Development* **141**, 2108-2118 (2014).

6. Bushati N, Stark A, Brennecke J, Cohen SM. Temporal reciprocity of miRNAs and their targets during the maternal-to-zygotic transition in Drosophila. *Current Biology* **18**, 501-506 (2008).

7. Schulz KN*, et al.* Zelda is differentially required for chromatin accessibility, transcription factor binding, and gene expression in the early Drosophila embryo. *Genome research* **25**, 1715-1726 (2015).

8. Dahanukar A, Walker JA, Wharton RP. Smaug, a novel RNA-binding protein that operates a translational switch in Drosophila. *Molecular cell* **4**, 209-218 (1999).

9. Hamm DC, Harrison MM. Regulatory principles governing the maternal-to-zygotic transition: insights from Drosophila melanogaster. *Open Biol* **8**, (2018).

10. Urieli-Shoval S, Gruenbaum Y, Sedat J, Razin A. The absence of detectable methylated bases in Drosophila melanogaster DNA. *FEBS letters* **146**, 148-152 (1982).

11. Simpson VJ, Johnson TE, Hammen RF. Caenorhabditis elegans DNA does not contain 5-methylcytosine at any time during development or aging. *Nucleic acids research* **14**, 6711-6719 (1986).

12. Jiang N, Wang L, Chen J, Wang L, Leach L, Luo Z. Conserved and Divergent Patterns of DNA Methylation in Higher Vertebrates. *Genome Biology and Evolution* **6**, 2998-3014 (2014).

13. Deaton AM, Bird A. CpG islands and the regulation of transcription. *Genes & development* **25**, 1010-1022 (2011).

14. Santos F, Hendrich B, Reik W, Dean W. Dynamic reprogramming of DNA methylation in the early mouse embryo. *Developmental biology* **241**, 172-182 (2002).

15. Yartseva V, Giraldez AJ. The Maternal-to-Zygotic Transition During Vertebrate Development: A Model for Reprogramming. *Current topics in developmental biology* **113**, 191-232 (2015).

16. Lyko F. The DNA methyltransferase family: a versatile toolkit for epigenetic regulation. *Nature Reviews Genetics* **19**, 81 (2018).

17. Bewick AJ, Vogel KJ, Moore AJ, Schmitz RJ. Evolution of DNA methylation across insects. *Molecular biology and evolution* **34**, 654-665 (2017).

18. Provataris P, Meusemann K, Niehuis O, Grath S, Misof B. Signatures of DNA methylation across insects suggest reduced DNA methylation levels in Holometabola. *Genome biology and evolution* **10**, 1185-1197 (2018).

19. Ventos-Alfonso A, Ylla G, Montanyes J-C, Belles X. DNA methylation in cockroaches is essential in early embryo development and reduces gene expression noise. *bioRxiv*, (2020).

20. Yi S. Birds do it, bees do it, worms and ciliates do it too: DNA methylation from unexpected corners of the tree of life. *Genome biology* **13**, (2012).

21. Bonasio R*, et al.* Genome-wide and caste-specific DNA methylomes of the ants Camponotus floridanus and Harpegnathos saltator. *Current Biology* **22**, 1755-1764 (2012).

22. Lyko F, Foret S, Kucharski R, Wolf S, Falckenhayn C, Maleszka R. The honey bee epigenomes: differential methylation of brain DNA in queens and workers. *PLoS biology* **8**, (2010).

23. Walsh TK*, et al.* A functional DNA methylation system in the pea aphid, Acyrthosiphon pisum. *Insect Molecular Biology* **19**, 215-228 (2010).

24. Bird A. Functions for DNA methylation in vertebrates. In: *Cold Spring Harbor Symposia on Quantitative Biology*). Cold Spring Harbor Laboratory Press (1993).

25. Keller TE, Han P, Yi SV. Evolutionary Transition of Promoter and Gene Body DNA Methylation across Invertebrate–Vertebrate Boundary. *Molecular Biology and Evolution* **33**, 1019-1028 (2016).

26. Zemach A, McDaniel IE, Silva P, Zilberman D. Genome-wide evolutionary analysis of eukaryotic DNA methylation. *Science* **328**, 916-919 (2010).

27. Sarda S, Zeng J, Hunt BG, Yi SV. The evolution of invertebrate gene body methylation. *Molecular biology and evolution* **29**, 1907-1916 (2012).

28. Hellman A, Chess A. Gene body-specific methylation on the active X chromosome. *science* **315**, 1141-1143 (2007).

29. Maunakea AK*, et al.* Conserved role of intragenic DNA methylation in regulating alternative promoters. *Nature* **466**, 253-257 (2010).

30. Hunt BG, Glastad KM, Yi SV, Goodisman MAD. The Function of Intragenic DNA Methylation: Insights from Insect Epigenomes. *Integr Comp Biol* **53**, 319-328 (2013).

31. Huh I, Zeng J, Park T, Yi SV. DNA methylation and transcriptional noise. *Epigenetics & Chromatin* **6**, (2013).

32. Smith ZD*, et al.* DNA methylation dynamics of the human preimplantation embryo. *Nature* **511**, 611-615 (2014).

33. Li L, Lu X, Dean J. The maternal to zygotic transition in mammals. *Molecular aspects of medicine* **34**, 919-938 (2013).

34. Guo H*, et al.* The DNA methylation landscape of human early embryos. *Nature* **511**, 606-610 (2014).

35. Bewick AJ, Sanchez Z, Mckinney EC, Moore AJ, Moore PJ, Schmitz RJ. Dnmt1 is essential for egg production and embryo viability in the large milkweed bug, Oncopeltus fasciatus. *Epigenetics & chromatin* **12**, 1-14 (2019).

36. Wang X*, et al.* Function and Evolution of DNA Methylation in Nasonia vitripennis. *PLoS Genetics* **9**, e1003872 (2013).

913 37. Park J*, et al.* Comparative analyses of DNA methylation and sequence
914 evolution using Nasonia genomes. *Molecular biology and evolution* **28**,
915 3345-3354 (2011).
916
917 38. Werren JH, Richards S, Desjardins CA, Niehuis O, Gadau J, Colbourne
918 JK. Functional and Evolutionary Insights from the Genomes of Three
919 Parasitoid *Nasonia* Species. *Science* **327**, 343-348 (2010).
920
921 39. Zwier M, Verhulst E, Zwahlen R, Beukeboom L, Van de Zande L. DNA
922 methylation plays a crucial role during early Nasonia development. *Insect*
923 *molecular biology* **21**, 129-138 (2012).
924
925 40. Lynch JA, Desplan C. A method for parental RNA interference in the wasp
926 Nasonia vitripennis. *Nat Protoc* **1**, 486-494 (2006).
927
928 41. Buchta T, Özüak O, Stappert D, Roth S, Lynch JA. Patterning the dorsal–
929 ventral axis of the wasp Nasonia vitripennis. *Developmental biology* **381**,
930 189-202 (2013).
931
932 42. Arsala D, Lynch JA. Ploidy has little effect on timing early embryonic
933 events in the haplo-diploid wasp Nasonia. *Genesis (New York, NY : 2000)*
934 **55**, (2017).
935
936 43. Liang H-L, Nien C-Y, Liu H-Y, Metzstein MM, Kirov N, Rushlow C. The
937 zinc-finger protein Zelda is a key activator of the early zygotic genome in
938 Drosophila. *Nature* **456**, 400-403 (2008).
939
940 44. Laver JD, Marsolais AJ, Smibert CA, Lipshitz HD. Regulation and
941 Function of Maternal Gene Products During the Maternal-to-Zygotic
942 Transition in Drosophila. *Current topics in developmental biology* **113**, 43-
943 84 (2015).
944
945 45. Arsala D, Wu X, Yi SV, Lynch JA. Supplemental item 1. (2020).
946
947 46. Wang Y*, et al.* Functional CpG methylation system in a social insect.
948 *Science* **314**, 645-647 (2006).
949
950 47. Wu X, Lindsey AR, Chatterjee P, Werren JH, Stouthamer R, Soojin VY.
951 Distinct epigenomic and transcriptomic modifications associated with
952 Wolbachia-mediated asexuality. *PLoS pathogens* **16**, e1008397 (2020).
953
954 48. Chen Z, Smith KR, Batterham P, Robin C. Smg1 nonsense mutations do
955 not abolish nonsense-mediated mRNA decay in Drosophila melanogaster.
956 *Genetics* **171**, 403-406 (2005).
957

958 49. Pulak R, Anderson P. mRNA surveillance by the Caenorhabditis elegans
959 smg genes. *Genes & development* **7**, 1885-1897 (1993).
960
961 50. McIlwain DR*, et al.* Smg1 is required for embryogenesis and regulates
962 diverse genes via alternative splicing coupled to nonsense-mediated
963 mRNA decay. *Proceedings of the National Academy of Sciences* **107**,
964 12186-12191 (2010).
965
966 51. Bhuvanagiri M*, et al.* 5-azacytidine inhibits nonsense-mediated decay in a
967 MYC-dependent fashion. *EMBO molecular medicine* **6**, 1593-1609 (2014).
968
969 52. Eckersley-Maslin MA, Alda-Catalinas C, Reik W. Dynamics of the
970 epigenetic landscape during the maternal-to-zygotic transition. *Nature*
971 *Reviews Molecular Cell Biology* **19**, 436-450 (2018).
972
973 53. Dunican DS, Ruzov A, Hackett JA, Meehan RR. xDnmt1 regulates
974 transcriptional silencing in pre-MBT Xenopus embryos independently of its
975 catalytic function. *Development* **135**, 1295-1302 (2008).
976
977 54. Seymour DK, Gaut BS. Phylogenetic Shifts in Gene Body Methylation
978 Correlate with Gene Expression and Reflect Trait Conservation. *Molecular*
979 *Biology and Evolution* **37**, 31-43 (2020).
980
981 55. Bewick AJ, Zhang YW, Wendte JM, Zhang XY, Schmitz RJ. Evolutionary
982 and Experimental Loss of Gene Body Methylation and Its Consequence to
983 Gene Expression. *G3-Genes Genom Genet* **9**, 2441-2445 (2019).
984
985 56. Takuno S, Seymour DK, Gaut BS. The Evolutionary Dynamics of
986 Orthologs That Shift in Gene Body Methylation between Arabidopsis
987 Species. *Molecular Biology and Evolution* **34**, 1479-1491 (2017).
988
989 57. Ventos-Alfonso A, Ylla G, Belles X. Zelda and the maternal-to-zygotic
990 transition in cockroaches. *The FEBS Journal* **286**, 3206-3221 (2019).
991
992 58. Washington JT, Cavender KR, Amukamara AU, McKinney EC, Schmitz
993 RJ, Moore PJ. The essential role of Dnmt1 in gametogenesis in the large
994 milkweed bug Oncopeltus fasciatus. *bioRxiv*, 2020.2007.2023.218180
995 (2020).
996
997 59. Schulz NK*, et al.* Dnmt1 has an essential function despite the absence of
998 CpG DNA methylation in the red flour beetle Tribolium castaneum.
999 *Scientific reports* **8**, 1-10 (2018).
1000
1001 60. Love MI, Huber W, Anders S. Moderated estimation of fold change and
1002 dispersion for RNA-seq data with DESeq2. *Genome biology* **15**, 550
1003 (2014).

61. Benjamini Y, Hochberg Y. Controlling the false discovery rate: a practical and powerful approach to multiple testing. *Journal of the Royal statistical society: series B (Methodological)* **57**, 289-300 (1995).

62. Hu H*, et al.* In-depth proteome of the hypopharyngeal glands of honeybee workers reveals highly activated protein and energy metabolism in priming the secretion of royal jelly. *Molecular & Cellular Proteomics* **18**, 606-621 (2019).

63. Park Y, Wu H. Differential methylation analysis for BS-seq data under general experimental design. *Bioinformatics* **32**, 1446-1453 (2016).